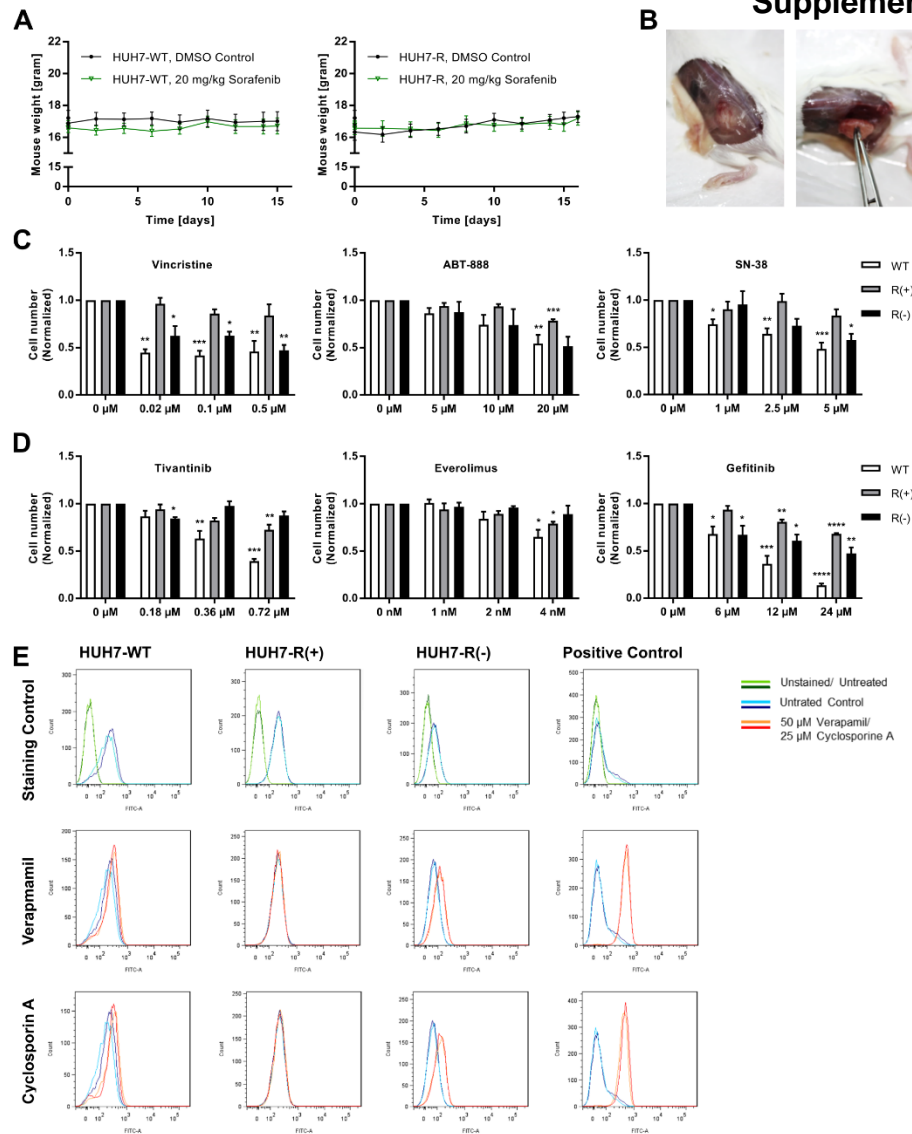


Supplemental figures:

Metabolic implication of tigecycline as an efficacious second-line treatment for sorafenib-resistant hepatocellular carcinoma

Supplemental Fig. S1



Supplemental Fig. S1. Cross-resistance obtained by HUH7-R(+) cells is independent of the MDR machinery.

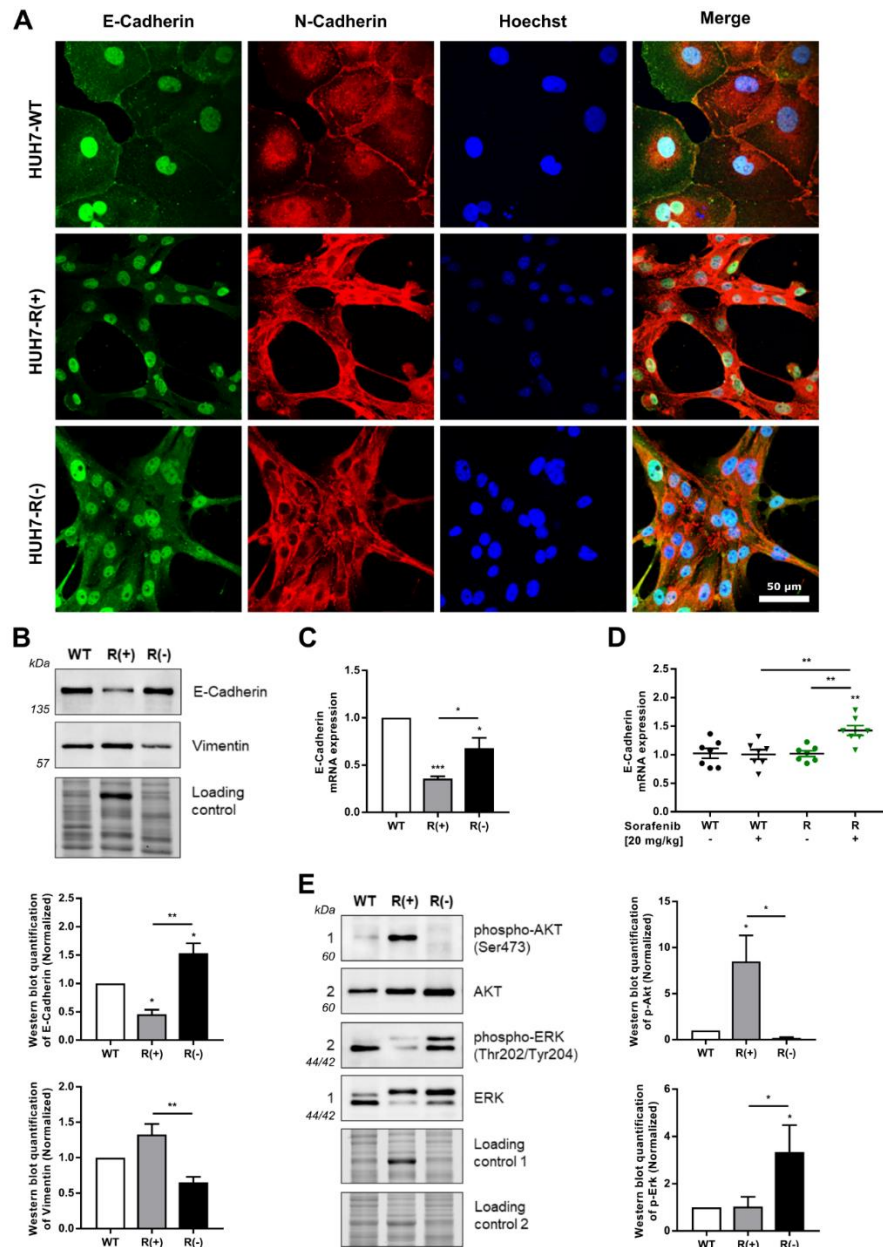
(A) Sorafenib therapy (20 mg/kg, every second day) of ectopic tumor mouse model (Fig. 1D) was well tolerated. The mouse weight was assessed at the indicated time points.

(B) HUH7-R cells show highly invasive tumor growth *in vivo*. Invasive growth of HUH7-R tumors in 4/7 mice of the Control group (DMSO) and 3/7 mice of the treated group (20 mg/kg sorafenib) (Fig. 1D).

(C) Acquired cross-resistance in HUH7-R(+) cells was also obtained for: chemotherapeutics as the microtubule-binding alkaloid vincristine, the PARP-inhibitor ABT-888, the topoisomerase I inhibitor SN-38 (ANOVA),

(D) the mTOR-inhibitor everolimus as well as the MET-, respective EGF-receptor inhibitors tivantinib and gefitinib. Proliferation rates within 72 h of treatment were normalized to the untreated control (ANOVA).

(E) The MDR-proteins P-glycoprotein (P-gp) and multidrug resistance protein (MRP) are not involved in the broad resistance-spectrum of HUH7-R(+) cells. Calcein retention was assessed by flow cytometry and MDR-positive vincristine-resistant CEM/VCR-R cells [5] were used as a positive control. Verapamil and cyclosporine A block MDR-transporters causing a shift in intracellular calcium retention. Values are shown as \pm SEM, N=7 for A-B, N=3 for C-E, * P <0.05, ** P <0.01, *** P <0.001, **** P <0.0001. Figure is related to Figure 1.



Supplemental Fig. S2. Sorafenib resistance is partially mediated by EMT and compensatory PI3K/Akt pathway activation.

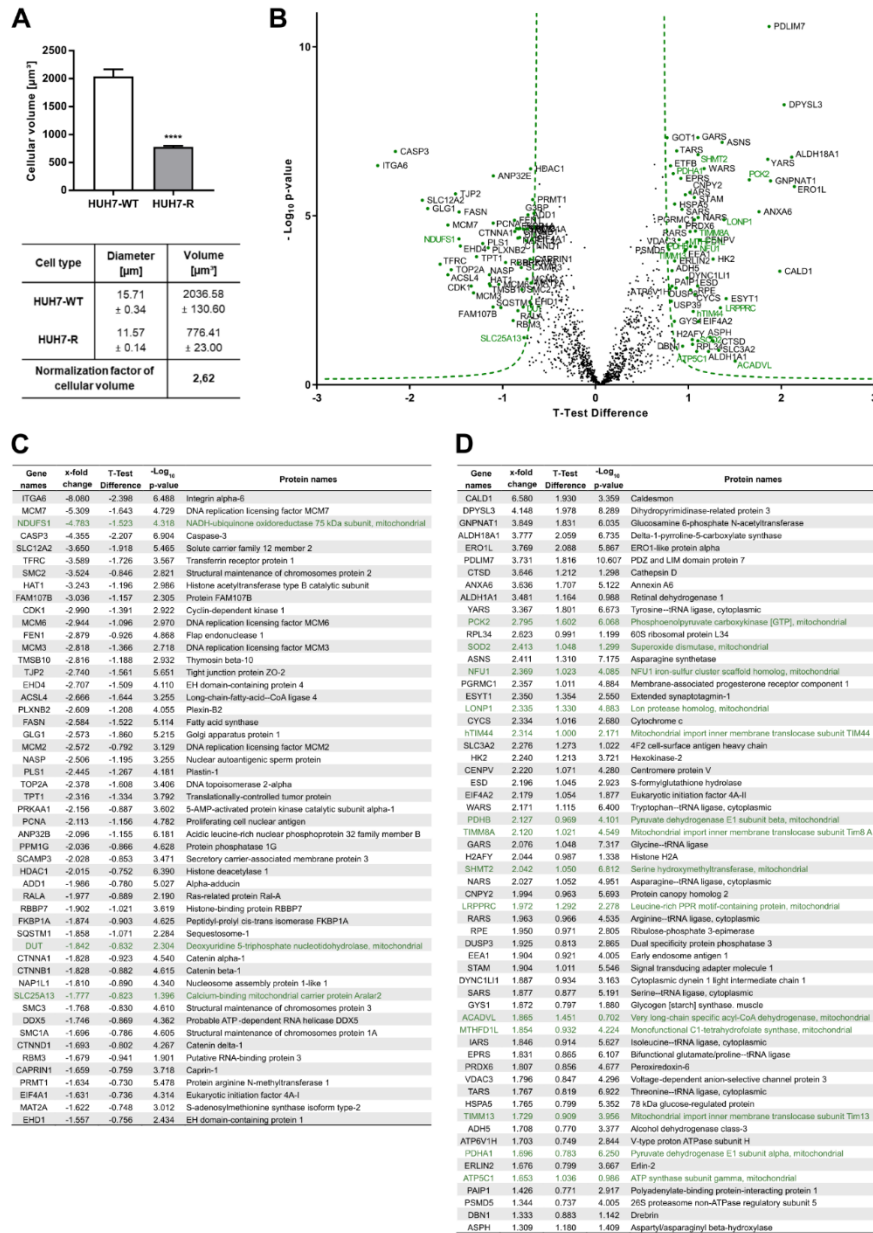
(A) Increased but reversible surface localization of N-Cadherin in HUH7-R(+) cells. Immunostaining of the EMT markers E-Cadherin (green), N-Cadherin (red) as well as Hoechst33342 (blue). Scale bar indicates 50 μ m.

(B) Long-term sorafenib exposure induces partial EMT in HUH7-R(+) cells. Quantitative immunoblot analysis of the EMT markers E-Cadherin and vimentin normalized to HUH7-WT (ANOVA).

(C) E-Cadherin mRNA-expression is regained upon rebound growth. E-Cadherin mRNA-levels were normalized to HUH7-WT (ANOVA).

(D) Sorafenib treatment modifies E-Cadherin mRNA-expression of HUH7-R cells *in vivo*. The E-Cadherin mRNA-levels of resected tumors (Fig. 1D) were normalized to the mean mRNA-expression of HUH7-WT (ANOVA).

(E) Evasive PI3K/Akt-signaling pathway is upregulated in HUH7-R(+) cells. Immunoblot quantification of phospho-AKT and phospho-ERK was normalized to HUH7-WT (ANOVA). Values are shown as \pm SEM, N=3 for A-C and E, N=7 for D, * P <0.05, ** P <0.01, *** P <0.001. Figure is related to Figure 1.



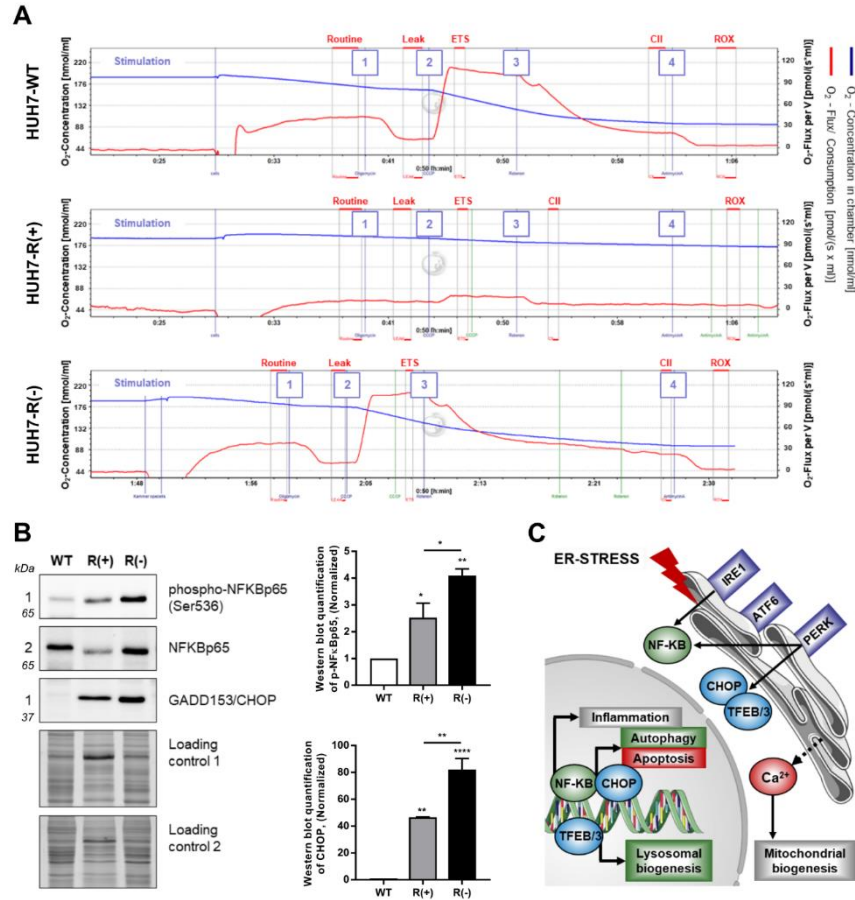
Supplemental Fig. S3. Volcano blot analysis of MS-proteomics screening compares HUH7-R(+) and HUH7-R(-) cells.

(A) HUH7-R cells have a significantly decreased cellular volume compared to HUH7-WT. The cellular diameter was assessed via image analysis by the ViCell cell counter and used for the calculation of the cellular volume (top). The ratio of cellular volume of HUH7-WT and HUH7-R cells results in a correction factor used for normalization of cellular fluorescent intensities obtained by flow cytometry, cellular ATP-levels and cellular oxygen consumption (bottom) (t-test).

(B) Volcano blot analysis. T-test Difference and $-\log_{10}$ p-value comparing the proteome of HUH7-R(+) and HUH7-R(-) are shown. Proteins lower and higher than the cut-off FDR 0.05, $s_0=2$ (dashed green line) are highlighted with green dots.

(C) Autophagic proteins and the mitochondrial Complex I (NDUFS1) are upregulated upon rebound growth. Proteins with a t-test Difference <-0.715 (higher abundance in HUH7-R(-)) from Supplemental Fig. S3B are listed according to their x-fold change.

(D) Mitochondrial proteins are downregulated upon rebound growth. Proteins with a t-test Difference >0.715 (higher abundance in HUH7-R(+)) from Supplemental Fig. S3B are listed according to their x-fold change. Proteins of mitochondrial origin are highlighted in green. Values are shown as \pm SEM, N=4 for A, N=5 with technical duplicates for B-D, **** $P<0.0001$. Figure is related to Figure 2.



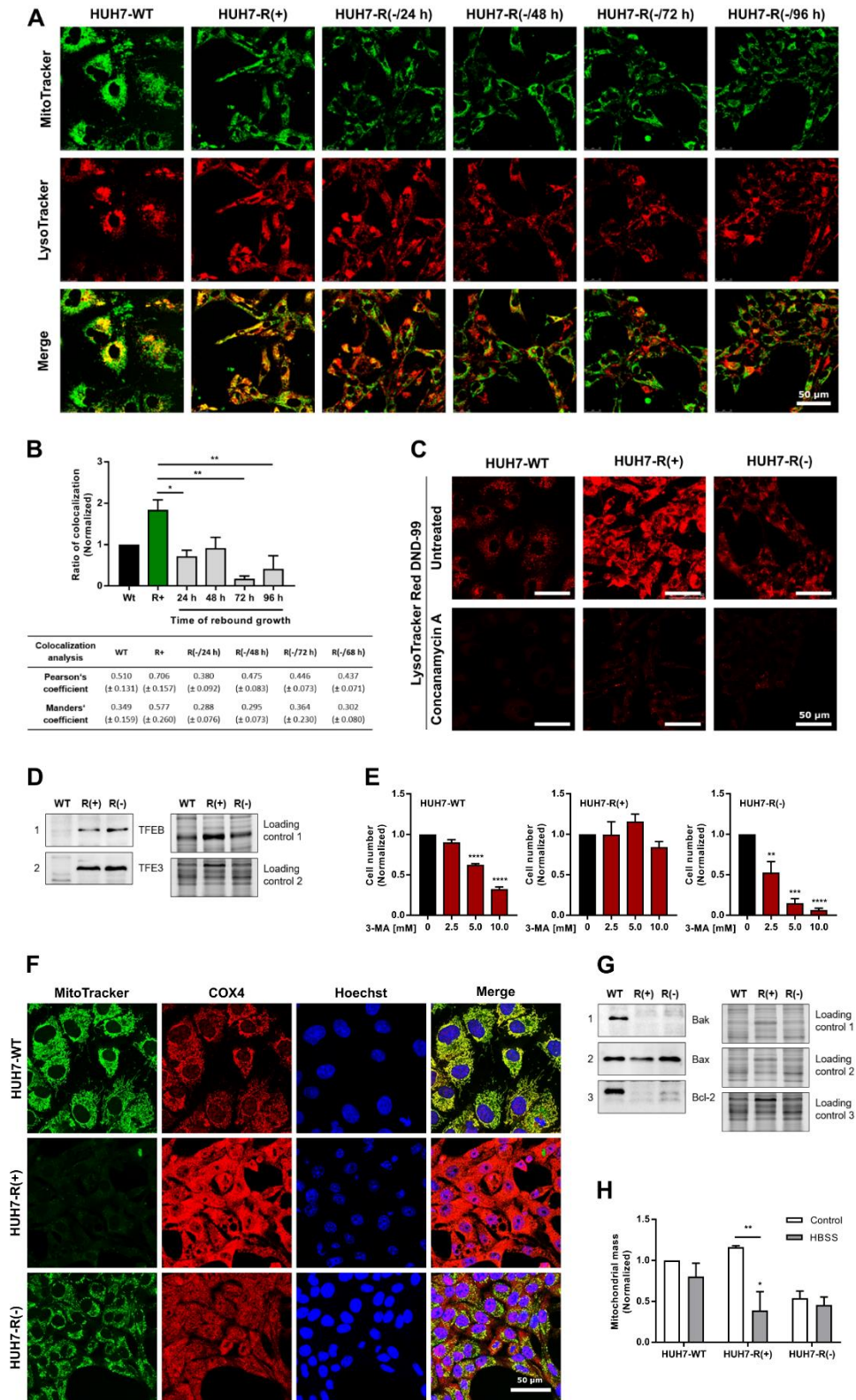
Supplemental Fig. S4. Mitochondrial damage and ER-stress.

(A) High-resolution respirometry. Representative O_2 -Flux over time measurements (red curves) of 1.6×10^6 HUH7-WT, HUH7-R(-) and 3.2×10^6 HUH7-R(+) cells are shown with the respective stimulation time points of oligomycin (400 μ M), CCCP (5 mM), rotenone (2 μ M) and antimycin A (500 μ M). For evaluation, the parameters Routine, Leak, ETS, Complex II and ROX were determined within the red segments. All parameters were normalized to the respective cell number.

(B) ER-stress pathways are strongly upregulated in HUH7-R cells. Quantitative immunoblot analysis of CHOP and NFKB-activation were normalized to HUH7-WT (ANOVA).

(C) ER-stress links Ca^{2+} -induced mitochondrial damage, activation of mitophagy and mitochondrial biogenesis in HUH7-R cells. Values are shown as \pm SEM, N=3, * P <0.05, ** P <0.01, **** P <0.0001. Figure is related to Figure 3.

Supplemental Fig. S5



Supplemental Fig. S5. Mitochondrial quality control pathways.

(A) Colocalization of mitochondria and lysosomes reduced upon sorafenib withdrawal. Colocalization (yellow) of MitoTracker (green) and LysoTracker (red) signals in merged images of live cell staining indicates mitophagy. MitoTracker and LysoTracker staining was performed in HUH7-WT, HUH7-R(+) cells and in HUH7-R cells upon 96 h of rebound growth. Scale bars indicate 50 μ m.

(B) Lysosomal translocation of damaged mitochondria might be induced in HUH7-R(+) cells. Colocalization of mitochondria and lysosomes was assessed by live cell imaging (*see Supplemental Fig. S5A*) and quantified via image analysis using the ImageJ software. The yellow area, which indicates mitophagy, was normalized to the total area of positive MitoTracker and LysoTracker signals. The calculated ratios of yellow to red and green area were normalized to the ratio obtained in HUH7-WT cells (upper panel). Pearson's and Manders' correlation coefficients for MitoTracker and LysoTracker signals were calculated as previously described (19, 20) (lower panel).

(C) Lysosomes are accumulated in HUH7-R(+) cells. LysoTracker staining and live cell imaging was performed for HUH7-WT, HUH7-R(+) and HUH7-R(-) cells. Concanamycin A (1 μ M) pretreatment for 4 h blocks lysosomal acidification and was used as a negative control. Scale bars indicate 50 μ m.

(D) Lysosomal biogenesis is activated in HUH7-R cells. Immunoblot analysis of the activators of lysosomal biogenesis TFEB and TFE3 is shown.

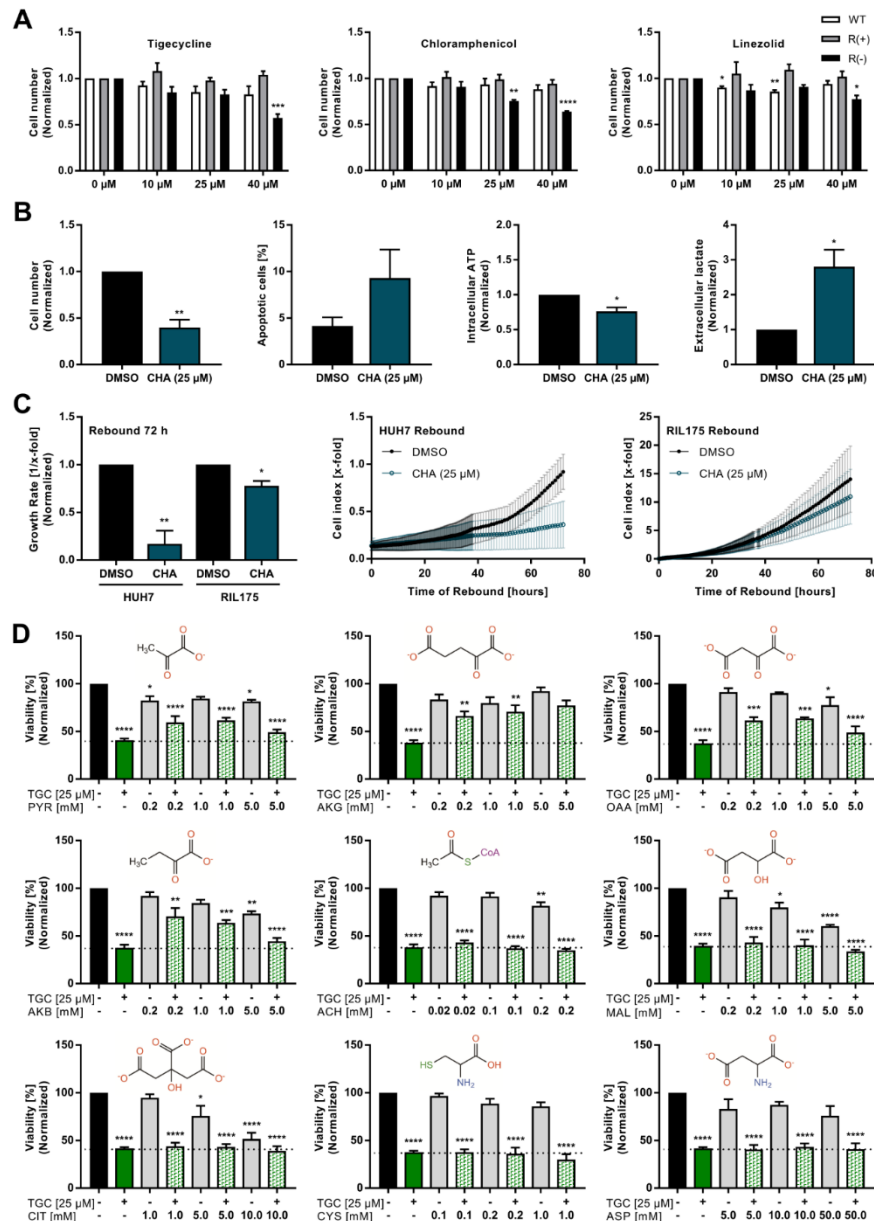
(E) Autophagic flux might be impaired in HUH7-R(+) cells. HUH7-WT, HUH7-R(+) and HUH7-R(-) cells were treated with the inhibitor of autophagosome formation 3-MA and cell number was assessed by crystal violet staining after 72 h of treatment. Cell numbers were normalized to the untreated control (ANOVA).

(F) Defect mitochondria accumulate in HUH7-R(+) cells, which are degraded upon growth resumption. Membrane potential dependent staining (MitoTracker, green) and immunostaining of COX4 (red) of the mitochondrial network after fixation are shown. Cell nuclei were stained with Hoechst33342 (blue). Scale bar indicates 50 μ m

(G) Degradation of OMM proteins in HUH7-R cells. Immunoblot analysis of apoptosis regulators Bak and Bcl-2, located on the OMM as well as the cytoplasmic protein Bak is shown.

(H) HUH7-R(+) cells have highest capacity of starvation-induced mitophagy. Cells were incubated with HBSS for 6 h before mitochondrial mass was assessed by flow cytometry and normalized to the untreated control of HUH7-WT (ANOVA). Values are shown as \pm SEM, N=3, * P <0.05, ** P <0.01. Figure is related to *Figure 3*.

Supplemental Fig. S6



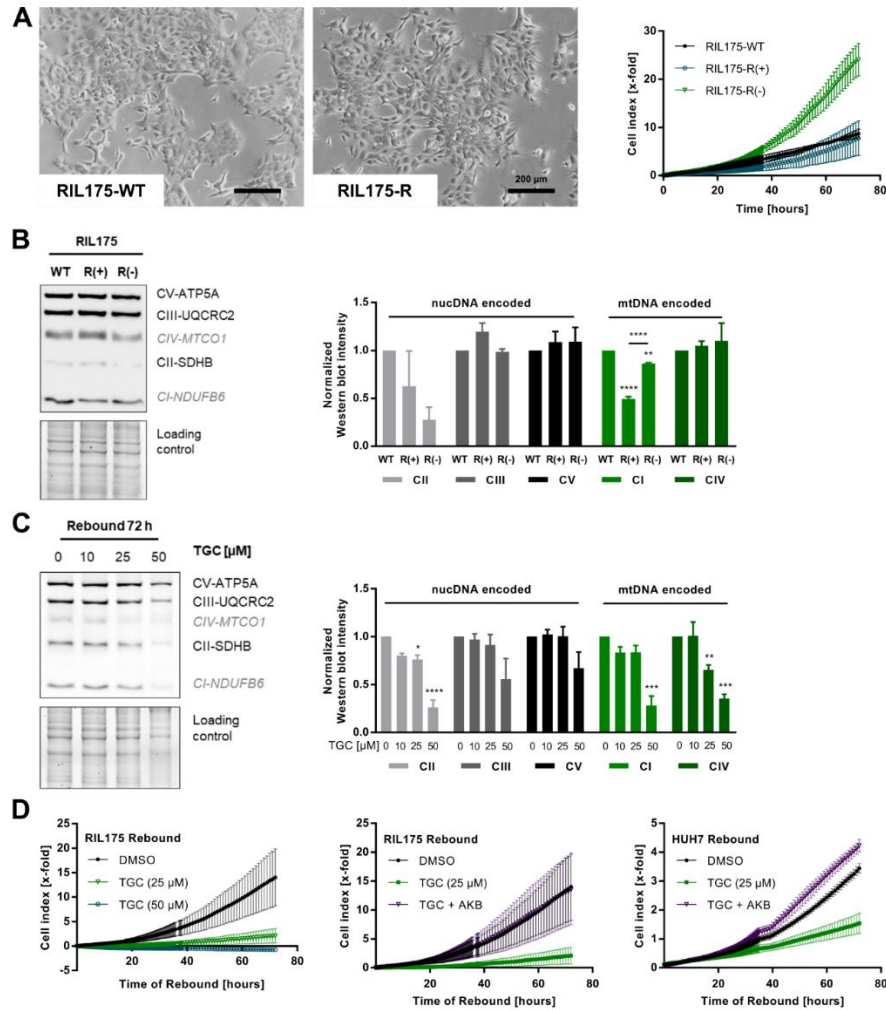
Supplemental Fig. S6. Translation-inhibiting antibiotics prevent rebound growth by limiting NAD⁺-recovery.

(A) Strongest reduction of cell number by treatment with the antibiotics tigecycline, chloramphenicol and linezolid was obtained in HUH7-R(-) cells. The cell number of HUH7-WT, HUH7-R(+) and HUH7-R(-) cells was assessed by crystal violet staining after 72 h of antibiotic treatment and normalized to the untreated control (ANOVA).

(B) The antibiotic CHA confirms the inhibition of tumor relapse second-line to sorafenib. Proliferation rate, apoptosis (percentage of whole cell count), intracellular ATP and extracellular lactate (all normalized to untreated control) of HUH7-R cells upon 72 h of rebound growth treated with chloramphenicol (CHA) (25 μ M) are shown (t-test).

(C) CHA shows more efficient inhibition of rebound growth in HUH7-R cells compared to RIL175-R cells. Growth rates of HUH7-R and RIL175-R cells upon 72 h of rebound growth were calculated from the normalized cell counts over time (cell index). The cell index was assessed by impedance measurement, and normalized to the DMSO control of the respective cell type (t-test).

(D) Exclusively alpha-keto acids rescue rebound growth upon TGC treatment. HUH7-R cells upon 72 h of rebound growth were treated with TGC and substituted with PYR, AKG, OAA, AKB, Acetyl-CoA (ACH), malate (MAL), citrate (CIT), cysteine (CYS) or aspartate (ASP). The viability was normalized to the untreated control (ANOVA). Values are shown as \pm SEM, N=3, * P <0.05, ** P <0.01, *** P <0.001, **** P <0.0001. Figure is related to Figure 5.



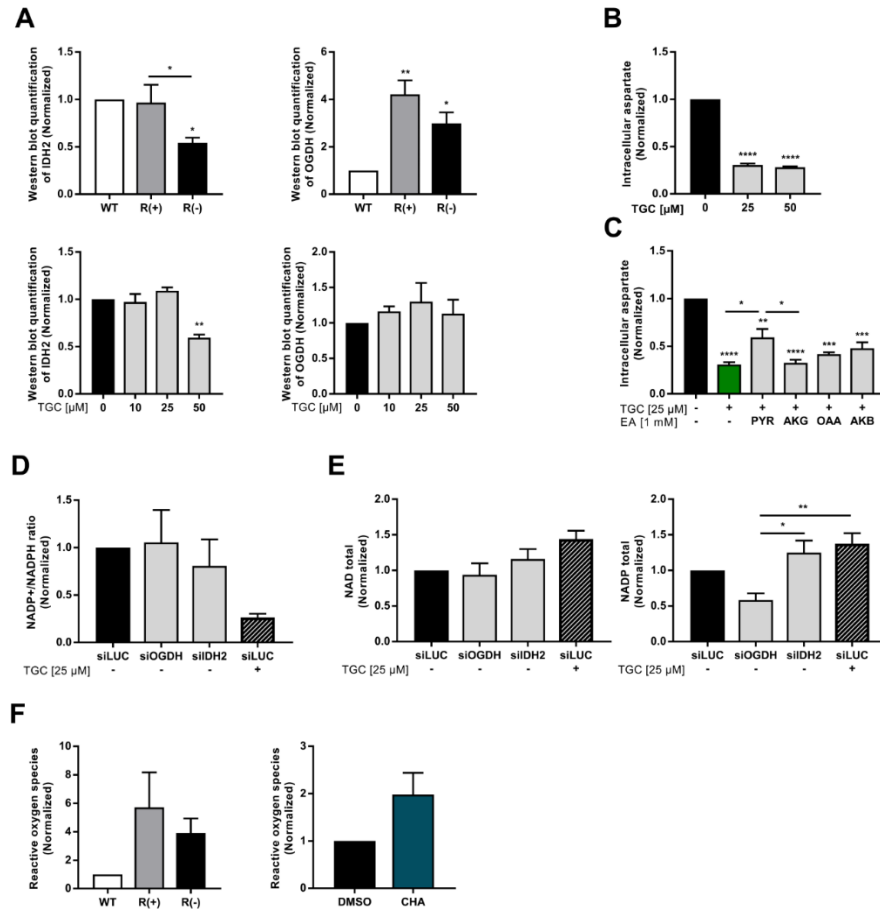
Supplemental Fig. S7. The sorafenib-resistant HCC rebound growth model with RIL175 cells.

(A) Sorafenib withdrawal from RIL175-R cells continuously cultured in 10 μM sorafenib (RIL175-R(+)) leads to significantly increased resumption of proliferation. Phase-contrast microscopy of wild-type (RIL175-WT) and sorafenib-resistant (RIL175-R) RIL-175 cells. Scale bars indicate 200 μm. Cells upon rebound growth were cultured, as already described for HUH7-R cells, without sorafenib for 72 h before seeding (RIL175-R(-)). Calculated growth rates of impedance measurements over 72 h are shown in Fig. 1E.

(B) Protein expression of NDUF is impaired in RIL175-R(+) cells and relapses upon sorafenib withdrawal. Immunoblot quantification of mtDNA- (CI-NDUFB6, CIV-MTCO1) and nucDNA-encoded ETS-subunits (CII-SDHB, CIII-UQCRC2, CV-ATP5A) was normalized to RIL175-WT (ANOVA).

(C) TGC inhibits the biogenesis of mtDNA-encoded ETS subunits. Immunoblot quantification of RIL175-R cells treated with TGC upon 72 h of sorafenib withdrawal (ANOVA).

(D) TGC impairs rebound growth of RIL175-R cells by establishing electron acceptor auxotrophy. TGC prevents rebound growth of RIL175-R cells comparable to HUH7-R cells, which is rescued by the exogenous electron acceptor AKB. Cells were treated with TGC respectively AKB upon sorafenib withdrawal and the proliferation was assessed by impedance measurement. Calculated growth rates over 72 h are shown in Fig. 5B (bottom) and Fig. 5D (right). Values are shown as ±SEM, N=3, **P*<0.05, ***P*<0.01, ****P*<0.001, *****P*<0.0001. Figure is related to Figure 1, Figure 3 and Figure 5.



Supplemental Fig. S8. Aspartate abundance is not limiting for rebound growth.

(A) OGDH expression is significantly upregulated in HUH7-R cells. Quantitative immunoblot analysis of IDH2 and OGDH (Fig. 6D) were normalized to HUH7-WT (left panels) or the untreated control (right panels) (ANOVA).

(B) TGC treatment strongly decreases the intracellular aspartate abundance. Intracellular aspartate levels were assessed for HUH7-R cells treated with TGC upon 72 h of rebound growth and normalized to the untreated control (ANOVA).

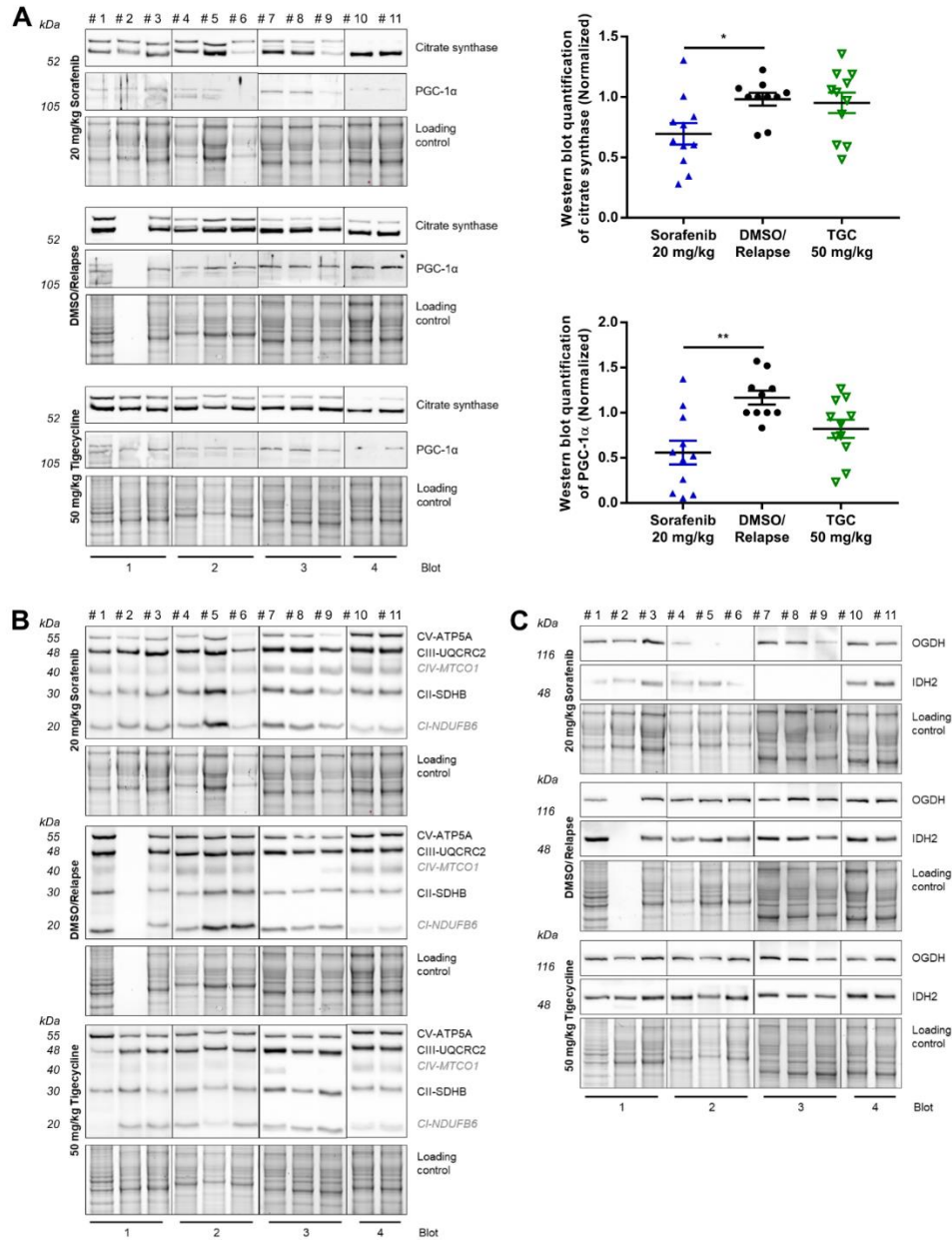
(C) Aspartate levels were not equally restored by substitution with EAs. HUH7-R cells upon 72 h of rebound growth were treated with TGC and the respective EA. Intracellular aspartate levels were normalized to the untreated control (ANOVA).

(D) The NADP⁺/NADPH ratio remains constant upon OGDH-silencing. HUH7-R cells upon 72 h of rebound growth were transfected with siLUC (Control), siOGDH or siIDH2 respectively treated with TGC. The NADP⁺/NADPH-ratio was normalized to the siLUC-transfected, untreated control (ANOVA).

(E) Biogenesis of NADP is sensitive to TCA-cycle inhibition. The total NAD and NADP levels of Fig. 6C and Supplemental Fig. S8D were assessed and normalized to the siLUC-transfected, untreated control (ANOVA).

(F) Increased ROS-production confirmed upon CHA (25 μ M) treatment. ROS-levels were normalized to HUH7-WT (upper panel) and to the untreated control (lower panel) (ANOVA). Values are shown as \pm SEM, N=3, * P <0.05, ** P <0.01, *** P <0.001, **** P <0.0001. Figure is related to Figure 6.

Supplemental Fig. S9

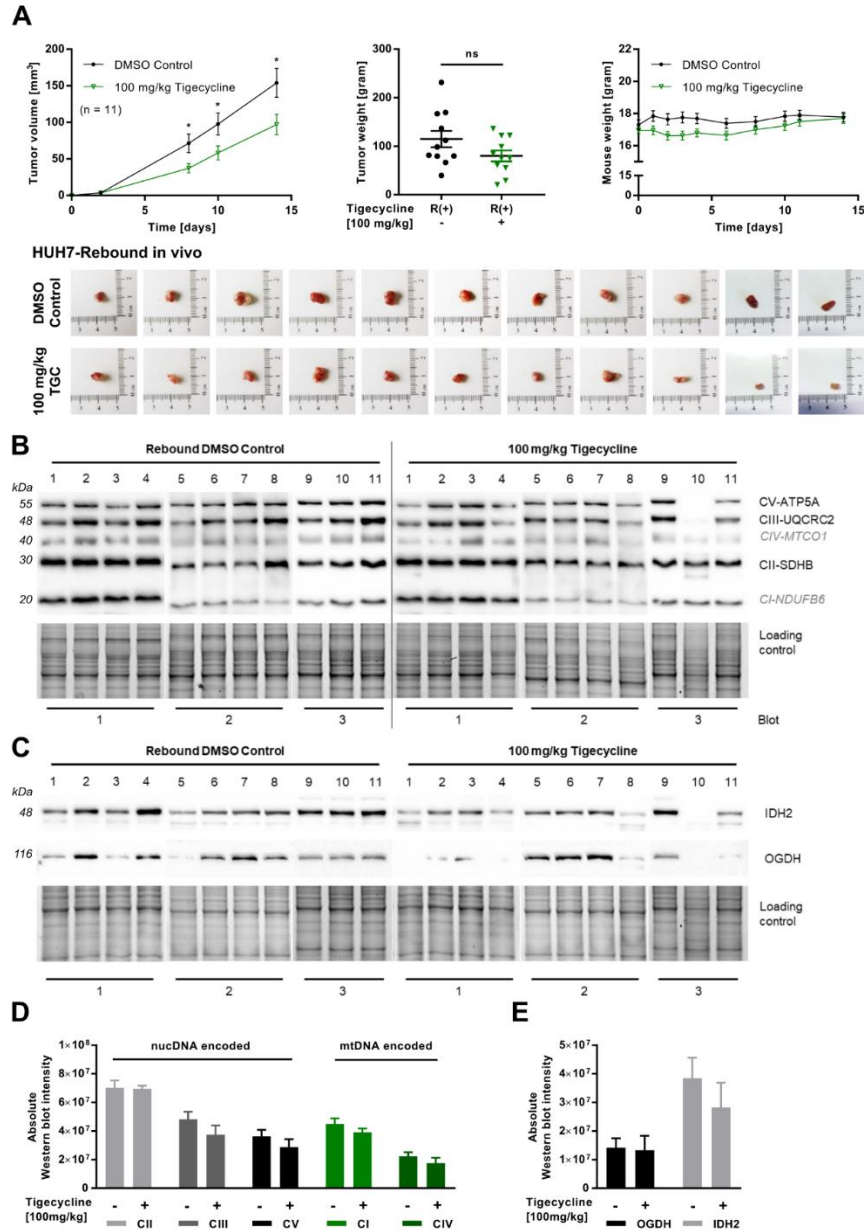


Supplemental Fig. S9. TGC treatment reduces CI-NDUFB6 protein expression *in vivo*.

(A) TGC treatment *in vivo* has a less pronounced effect on mitochondrial dynamics than sorafenib. Immunoblot analysis of excised tumors from ectopic tumor mouse model (Fig. 7) for citrate synthase (marker for mitochondrial mass) and the transcriptional regulator of mitochondrial biogenesis PGC-1 α is shown (left panel). Immunoblot quantifications (right panels) were normalized to the mean band intensities (ANOVA). Values are shown as \pm SEM, N=3, * P <0.05, ** P <0.01.

(B) TGC diminishes the protein expression of the CI-NDUFB6 subunit *in vivo*. Immunoblot analysis of excised tumors from ectopic tumor mouse model (Fig. 7) for mtDNA- (CI-NDUFB6, CIV-MTCO1) and nucDNA-encoded subunits (CII-SDHB, CIII UQCRC2, CV ATP5A) is shown.

(C) IDH2 and OGDH protein expression elevated upon tumor relapse. Immunoblot analysis of excised tumors from ectopic tumor mouse model (Fig. 7) is shown. Figure is related to Figure 7.



Supplemental Fig. S10. TGC shows strongest inhibition of tumor relapse in initial phase.

(A) TGC significantly inhibits tumor relapse under long-term treatment. Ectopic tumor mouse xenograft of HUH7-R(+) cells upon sorafenib withdrawal *in vivo*. Mice were left untreated (DMSO) or treated with TGC (100 mg/kg) every second day for 14 days. The resected tumors at day 14 are shown (t-test).

(B) TGC has no effect on protein expression of ETS subunits under long-term treatment. Immunoblot analysis of excised tumors from ectopic tumor mouse model (*Supplemental Fig. S10A*) for mtDNA- (CI-NDUFB6, CIV-MTCO1) and nucDNA-encoded subunits (CII-SDHB, CIII-UQCRC2, CV-ATP5A) is shown.

(C) TGC has no effect on protein expression of IDH2 and OGDH under long-term treatment. Immunoblot analysis of excised tumors (*Supplemental Fig. S10A*) is shown.

(D) Quantification of protein expression (*Supplemental Fig. S10B*) of mtDNA- and nucDNA-encoded ETS-subunits (ANOVA).

(E) Quantification of protein expression (*Supplemental Fig. S10C*) of IDH2 and OGDH (ANOVA). Values are shown as \pm SEM, N=11, * P <0.05. Figure is related to Figure 7.